Modelling of plasma discharge in a filament negative ion source

Modelling of plasma discharge in a filament negative ion source

V Candeloro[1], E Sartori[2], M Kisaki[3], M Kashiwagi[3], H Tobari[3], G Serianni[1]

[1]Consorzio RFX (CNR, ENEA, INFN, University of Padua, Acciaierie Venete S.p.A.), Corso Stati Uniti 4, 35127 Padova, Italy
[2]University of Padua – Department of Management and Engineering (DTG), Stradella S. Nicola 3, 36100 Vicenza, Italy
[3]National Institutes for Quantum Science and Technology (QST), Naka, Ibaraki, Japan

Corresponding author: Valeria Candeloro valeria.candeloro@igi.cnr.it

Abstract. Most of the currently operating Negative ion Neutral Beam Injectors (N-NBIs) exploit filament powered sources for the generation of beam ions. Being widely used in fusion experiments, the filament arc technology has been thoroughly investigated and optimized over the years, allowing to achieve excellent performances in terms of extracted beam optics. The source geometry, the magnetic field topology and the arc power strongly influence both the plasma discharge and the background gas properties and, consequently, the beam features. In this framework, this contribution describes a numerical investigation of the plasma properties in a filament-powered negative ion source, performed by means of a 2D3V Particle In Cell-Monte Carlo Collisions (PIC-MCC) code. Specifically, we discuss plasma formation by the thermionic electrons emitted by the filaments, investigating their interaction with the background gas. We also study the plasma diffusion through the magnetic filter field and how the latter modifies plasma density, electron temperature and plasma potential along the axial direction when approaching the plasma facing electrode.

1. Introduction

Filament-arc negative ion sources have been widely investigated and used for Negative ion Neutral Beam Injection (NNBI) systems [1], as opposed to Radio-Frequency (RF) sources, on which the R&D activities have more recently started. Filament sources are capable of delivering high current negative ion beams at 1 MeV energy with 3 mrad divergence, as demonstrated in the Megavolt Test Facility at QST [2]. A minimum divergence of 12 mrad was achieved in the ITER ion source prototype with 42 keV beam energy [3]. In filament-arc sources, plasma ignition is based on electron thermionic emission by hot (T∝1000 K) filaments. In order to maximize the background gas ionization efficiency, these sources are provided with a multi-cusp magnetic confinement on all the chamber surfaces. An example of this design, called Kamaboko ion source, was first developed by the Japan Atomic Energy Research Institute and operated on the MANTIS test facility, in France [4]. Permanent magnets are also used for generating the magnetic filter field, aimed at reducing the electron temperature in the proximity of the extraction region for avoiding the destruction of surface-produced negative ions.
With the aim of understanding what are the source plasma features at the basis of the better performances of filament sources, a bidimensional numerical investigation based on self-consistent PIC simulations has been carried out, focussing on the role of neutrals in the discharge and the equilibrium and dynamics of the ion species.

2. Simulation model

A 2D3V PIC-MCC code [5] was applied for investigating filament-based hydrogen plasma discharges, taking as reference the negative ion source hosted at QST-MTF. The simulation domain lies on a two-dimensional plane horizontally cutting the ion source, as shown in Figure 1. The chamber inner surfaces are represented as plain metallic walls and are grounded. The bottom wall represents the PG electrode and is polarized at $V_{BI} = 2\text{V}$ with respect to the other surfaces. The multi-cusp magnetic field is generated by a set of 14 permanent magnets placed on the round wall with regular spacing. The magnetic filter field is generated by two additional magnets placed close to the extraction region.

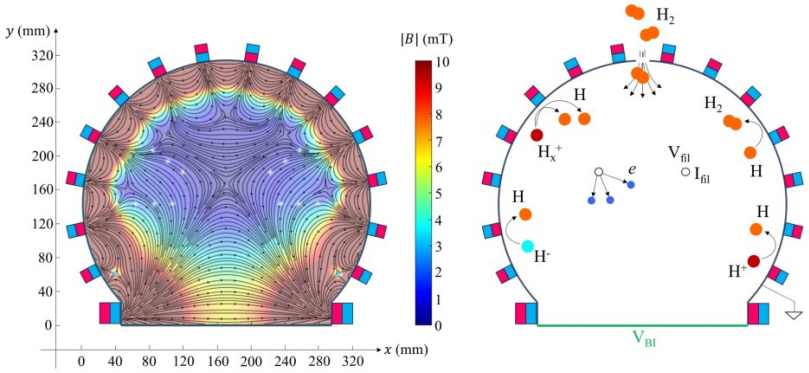

Figure 1. On the left: simulated magnetic field topology; on the right: simulation domain and schematic representation of the main features: gas injection, thermionic emission, plasma-wall interaction processes.

The considered species are electrons e, positive ions H^+, H_2^+, H_3^+, negative ions H^-, and neutral atoms H and molecules H_2, all kinetically described. Neutral H_2 molecules are injected from a 10 mm wide aperture in the upper section of the round walls. The number of molecules to be injected at each iteration is obtained as $N_{H2} = \Gamma_{H2} A_{inj} dt$, where dt is the simulation timestep, A_{inj} is the injection area and the flux Γ_{H2} is defined as:

$$\Gamma_{H_2} = 0.25 n_{eq} v = 0.25 \frac{p_{eq}}{k_B T_{room}} \left(\frac{8 k_B T_{room}}{\pi m_{H_2}} \right)^{0.5} \quad (1)$$

with p_{eq} and T_{room} being the target gas pressure and room temperature respectively. For the simulations shown in this work, no collisions between neutral particles were included. In the real source, filaments are radially oriented; nonetheless, reproducing the same geometry within the simulation would have caused most of the electrons to be emitted with a non-negligible velocity component along the non-simulated direction. For this reason, it was decided to include the filaments as two small circles of 2.5 mm placed at roughly 200 mm height with respect to the PG, with their position being symmetric with respect to the vertical direction. The filament bias V_{fil}=-80V and current I_{fil}=280A are defined in such a way to deliver an arc power per unit length of 45 kW/m, comparable to the real case. Other simulation parameters are listed in Table 1.

The domain is initially filled with H_2 molecules until a stationary state is reached. At this point, electron emission from the hot filaments begins, starting the plasma discharge. The system then evolves self-consistently towards a new stationary state as a result of the included collision processes, of plasma-wall interaction (Y_{rec}=0.12), and of thermionic emission, having fixed the operating gas pressure and the arc power. Two different cases are discussed, namely one with gas filling pressure 0.3Pa, and the other one with pressure 0.6Pa. All other parameters were left unchanged.

Table 1. Main simulation parameters.

Parameter	Description	Value	Parameter	Description	Value
β	Density scaling factor	0.0001	dt_{gas}	timestep for gas solution	5 ns
dx=dy	Unit cell size	0.8 mm	dt	timestep for plasma solution	1 ns

3. Evolution of neutral background

The time evolution of the number of simulated particles, N_{MP}, their rates, and temperature averaged over the entire domain are shown in Figures 2 and 3 for 0.3 and 0.6 Pa pressure respectively. In the low pressure case, three different phases are shown, namely (i) only gas, during which only H_2 molecules were injected, (ii) plasma phase, when thermionic emission was enabled, and (iii) last phase in which Coulomb collision between positive ions were included. Both at plasma ignition and when the background gas pressure is increased to 0.6 Pa (i.e. the number of injected H_2 molecules per timestep is doubled), the number of e and H_2^+ ions grows exponentially and, at the same time, the number of molecules decreases due to background gas ionization. The numbers of both H^+ ions and atoms start growing after some time, that is when dissociation starts. As can be seen from Figure 2, Coulomb collisions between positive ions causes a significant reduction of their average temperature.

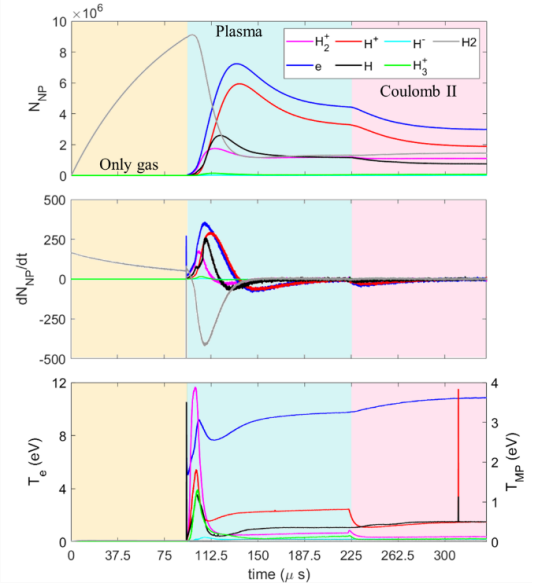

Figure 2. From top to bottom: number of simulated particles N_{MP} , their rates dN_{MP}/dt, and average temperature T_{MP} (T_e on left axis, other species on right axis) as a function of the simulated time. The three phases are highlighted, namely (i) only gas in yellow, (ii) plasma in light blue, and (iii) Coulomb collisions between positive ions in pink. Background gas pressure: 0.3 Pa.

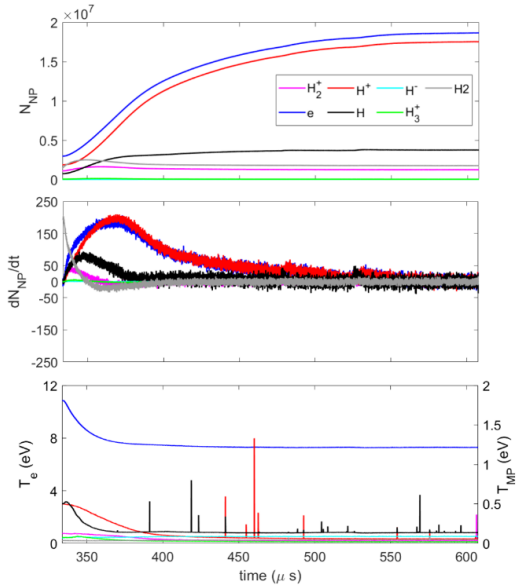

Figure 3. From top to bottom: number of simulated particles N_{MP}, their rates dN_{MP}/dt, and average temperature T_{MP} (T_e on left axis, other species on right axis) as a function of the simulated time. Background gas pressure: 0.6 Pa. The simulation started from the Coulomb II phase obtained at 0.3 Pa with increased H_2 injection.

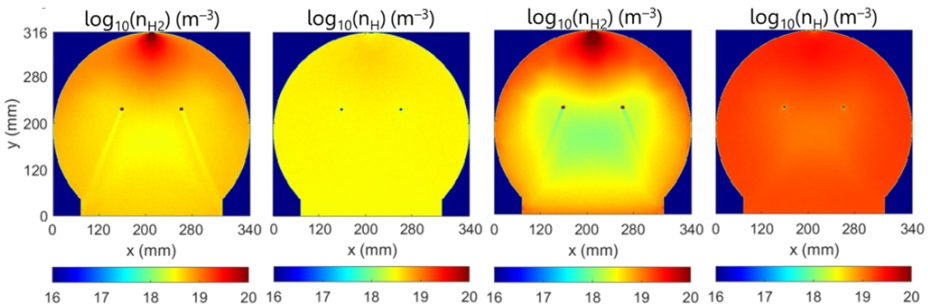

Figure 4. Two-dimensional H_2 and H density maps for low (first two subplots) and high (last two subplots) background gas pressure values.

Figure 4 shows the two-dimensional maps of H_2 and H densities in a stationary state for both low and high background gas pressures. Neutral depletion is clearly visible in the central region of the simulation domain, where the H_2 density drops of about one order of magnitude with respect to the density in the injection region. At the same time, the H density increases up to roughly 1×10^{19} m^{-3}, comparable with the molecular density. As expected, this phenomenon is much more evident for higher background gas pressure. In particular, the atom density at the centre of the chamber becomes dominant over the molecular density.

4. Plasma properties with low and high background gas pressure

The plasma density at the center of the discharge volume obtained in the 0.3 Pa case is roughly 1.5×10^{18} m^{-3}, as can be seen from Figure 5. The plasma potential is positive, but still very low.

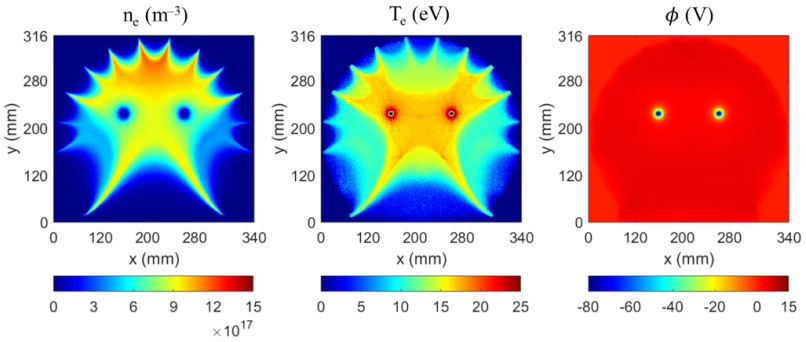

Figure 5. Two-dimensional maps of electron density, electron temperature and plasma potential for a stationary state at 0.3 Pa background gas pressure.

By doubling the injected H_2 flow, the plasma density is tripled with respect to the low pressure case. At the same time, the plasma potential is increased of a few V, whereas the electron temperature between the filaments decreases of roughly 5-7 eV with respect to the low pressure case.

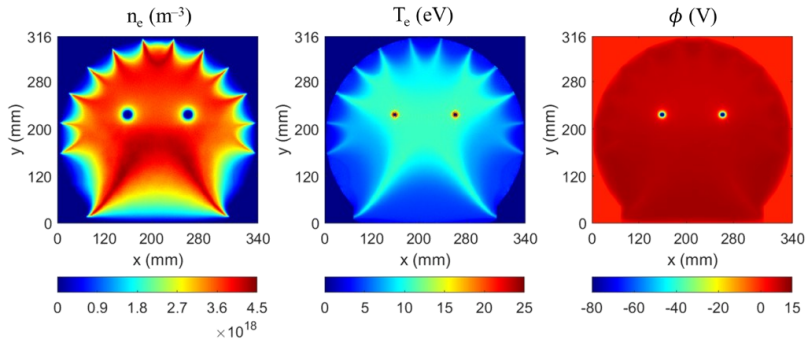

Figure 6. Two-dimensional maps of electron density, electron temperature and plasma potential for a stationary state at 0.6 Pa background gas pressure.

Figure 7 shows the vertical axial profiles of electron density, temperature, and plasma potential, for both the low and high background gas pressure values. The most evident difference is the plasma density in the proximity of the PG electrode. In the low pressure case, the density value at the PG is very low, of the order of 10^{16} m^{-3}, whereas in the high pressure case it becomes much larger. This might be explained by the reduction of the electron temperature in correspondence of the peak density: in fact, less energetic electrons are more likely to diffuse across the perpendicular magnetic field. However, the electron temperature in the proximity of the PG electrode is the same for both cases, which is around 4 eV. This rather high value might imply that some collisional processes are still missing; for instance, electrons might lose some energy due to either vibrational or rotational excitation of the background molecules,

which is not currently included in this model. The plasma potential close to the PG electrode, which is biased at 2 V, is doubled in the high pressure case.

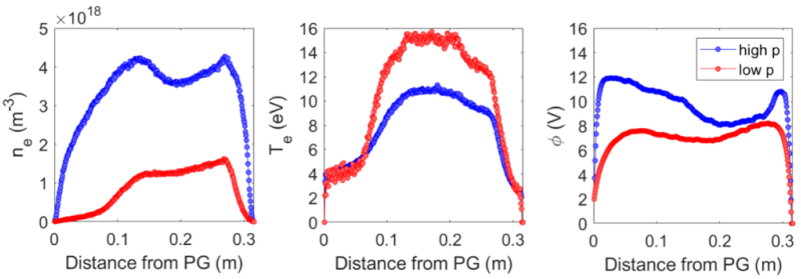

Figure 7. From left to right: electron density n_e, electron temperature T_e, and plasma potential φ for the low (red) and high (blue) background gas pressure cases.

5. Dissociation degree and positive ion effective mass

The total background gas dissociation degree $\delta = n_{\mathrm{H}}/(n_{\mathrm{H}} + n_{\mathrm{H}_2})$ and the positive ion effective mass $m_{\mathrm{eff}} = (n_{H^+} + 2n_{H_2^+} + 3n_{H_3^+})/(n_{H^+} + n_{H_2^+} + n_{H_3^+})$ can be obtained from the simulations. The results are shown in Figure 8 for both low and high pressure cases. When increasing the background gas pressure, the average dissociation degree increases from 0.52 to 0.75; coherently, the positive ion effective mass decreases from $1.23m_{\mathrm{H}^+}$ to $1.07m_{\mathrm{H}^+}$. In both cases, the background gas dissociation degree is larger than 50%, causing the ion effective mass to be very close to the proton mass, especially in the high pressure case. As expected, δ is higher where the neutral depletion takes place, whereas in the proximity of the chamber surfaces it becomes lower due to wall recombination. The ion effective mass is lower in the bottom half of the plasma chamber, underneath the two filaments. This effect is more visible in the high pressure case.

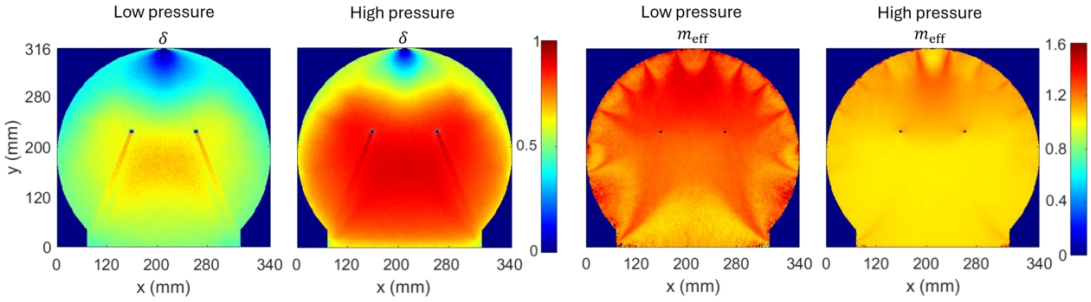

Figure 8. Two-dimensional maps of total dissociation degree and positive ion effective mass for low and high background gas pressure.

6. Conclusions

A first numerical characterization of the plasma discharge in a kamaboko-type negative ion source was presented. The motivation of this study stems from the fact that, with the same accelerator design, filament-based sources provide better performances in terms of beam divergence. This difference is related to the plasma properties in the ion source, more precisely to the behavior of the fast atoms and positive ions, which are the precursor species for surface produced negative ions. The simulation was proven to be capable of reaching a reasonable stationary state given only four input parameters: background gas pressure, arc current, filament bias, and PG bias voltage. Two cases at different pressures were compared: as expected, by increasing the gas pressure the plasma density and potential increase as well, whereas the electron temperature decreases. The higher pressure value causes the ion effective mass to be very close to the proton mass, also yielding a larger dissociation fraction, which is higher than 50% both simulated cases.

7. References

[1] Kuryiama M et al 1998 J. Nucl. Sci. Technol. 35
[2] Kashiwagi M et al 2022 Rev. Sci. Instrum. 93 053301
[3] Sartori E et al 2023 Nucl. Fus. 62
[4] Pamela J et al 1995 Rev. Sci. Instrum. 26
[5] Candeloro V, Sartori E, Serianni G 2023 JINST 18 C06028

Acknowledgments
This work has been carried out within the framework of the EUROfusion Consortium, funded by the European Union via the Euratom Research and Training Programme (Grant Agreement No 101052200 EUROfusion). Views and opinions expressed are however those of the author(s) only and do not necessarily reflect those of the European Union or the European Commission. Neither the European Union nor the European Commission can be held responsible for them.